

GaMeS: Mesh-Based Adapting and Modification of Gaussian Splatting

Joanna Waczyńska^{1*} Piotr Borycki^{1*} Sławomir Tadeja² Jacek Tabor¹ Przemysław Spurek¹

Abstract

In recent years, a range of neural network-based methods for image rendering have been introduced. For instance, widely-researched neural radiance fields (NeRF) rely on a neural network to represent 3D scenes, allowing for realistic view synthesis from a small number of 2D images. However, most NeRF models are constrained by long training and inference times. In comparison, Gaussian Splatting (GS) is a novel, state-of-the-art technique for rendering points in a 3D scene by approximating their contribution to image pixels through Gaussian distributions, warranting fast training and swift, real-time rendering. A drawback of GS is the absence of a well-defined approach for its conditioning due to the necessity to condition several hundred thousand Gaussian components. To solve this, we introduce *Gaussian Mesh Splatting* (GaMeS) model, a hybrid of mesh and a Gaussian distribution, that pin all Gaussians splats on the object surface (mesh). The unique contribution of our methods is defining Gaussian splats solely based on their location on the mesh, allowing for automatic adjustments in position, scale, and rotation during animation. As a result, we obtain high-quality renders in the real-time generation of high-quality views. Furthermore, we demonstrate that in the absence of a predefined mesh, it is possible to fine-tune the initial mesh during the learning process.

1. Introduction

Recently, we have observed the emergence of several promising methods for rendering unseen views of 3D objects and scenes using neural networks. For instance, Neural Radiance Fields (NeRFs) (Mildenhall et al., 2020) have

^{*}Equal contribution ¹Jagiellonian University, Faculty of Mathematics and Computer Science, Cracow, Poland ²Department of Engineering, University of Cambridge, Cambridge, UK. Correspondence to: Joanna Waczyńska <joanna.waczynska@doctoral.uj.edu.pl>.

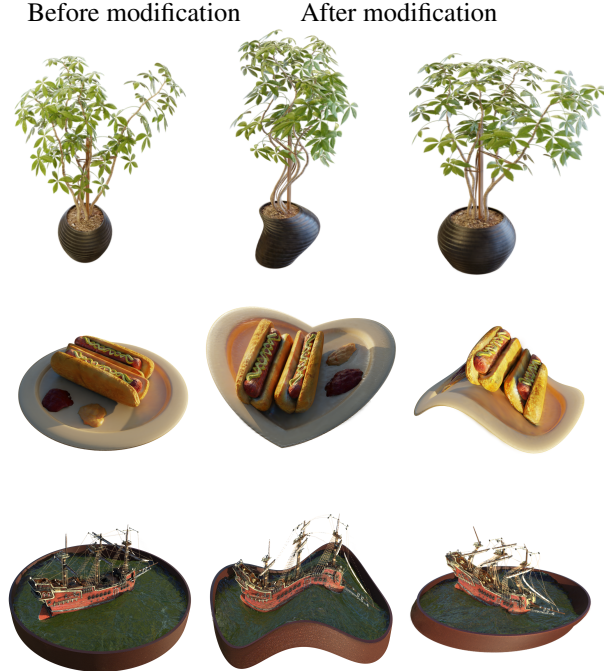


Figure 1. GaMeS produce a hybrid of Gaussian Splatting and mesh representations. Therefore, GaMeS allows real-time modification and adaptation of Gaussian Splatting. The supplementary material provides more examples, including a video illustrating our results.

rapidly grown in popularity within the computer vision and graphics community (Gao et al., 2022) as they enable the creation of high-quality renders. Despite this interest and growing body of related research, the long training and inference time remains an unsolved challenge for NeRFs.

In contrast, latterly introduced Gaussian Splatting (GS) (Kerbl et al., 2023) offers swift training and real-time rendering capabilities. What is unique to this method is that it represents 3D objects using Gaussian distributions (i.e. Gaussians). Hence, it does not rely on any neural network. Consequently, Gaussians can be employed in a manner akin to manipulating 3D point clouds or meshes, allowing for actions like resizing or repositioning in 3D space. Nonetheless, practical challenges may arise when altering Gaussian positions, particularly in accurately tracking changes in the shape of Gaussian components, such as the

ellipses. Moreover, scaling Gaussian components proves challenging when the object undergoes resizing, which is not an issue for classical meshes, as their triangle faces can be readily updated when vertex positions are adjusted.

The above constraints may be resolved by constructing Gaussian directly on the mesh, as shown by SuGaR (Guédon & Lepetit, 2023). Here, the authors introduced a regularization term in the Gaussian splat cost function to promote optimal alignment of the Gaussians with the scene’s surface. SuGaR uses signed distance functions (SDF) from the vanilla GS and minimizes the difference between this SDF and its actual value computed for the Gaussians. In SuGaR, the authors propose a method for extracting mesh from the GS model. They also introduce an optional refinement strategy that binds Gaussians to the surface of the mesh and jointly optimizes these Gaussians and the mesh through GS rendering.



Figure 2. GaMeS can be effectively trained on large scenes to allow their modifications while preserving high-quality renders.

We claim that the third stage of SuGaR can be seen as a separate method and trained from simple mesh initialization or when we have the given mesh. In our paper, we modify the refinement strategy from SuGaR.

To address this postulate, we introduce a modification of SuGeR refinement strategy called *Gaussian Mesh Splatting* (GaMeS), combining the concepts of mesh and Gaussian distribution. Implementing the GaMeS involves positioning Gaussian components on the faces of the mesh, ensuring proper alignment of these components with the mesh structure. Using our methodology, we can obtain comparable to state-of-the-art high-quality outcomes that can be attained

for static scenes, akin to the SuGeR method. Moreover, any alterations applied to the mesh will automatically propagate updates to the corresponding Gaussian components, enabling real-time animation, see Fig. 1. Our approach can be applied in scenarios with pre-existing mesh that we do not want to modify during the training, or requiring simultaneous optimization of both the mesh and Gaussian Splatting, see Fig. 2. In summary, this work makes the following contributions:

- We show that the refinement strategy from SuGaR can be trained without expensive mesh fitting.
- We introduce a hybrid representation for 3D objects, seamlessly integrating mesh and GS.
- Our method relies only upon basic vector operation, and consequently, we are able to render dynamic scenes at a similar time to their static counterpart.

2. Related Works

Point-based Gaussian representations have found a large number of potential application scenarios, including substituting point-cloud data (Eckart et al., 2016), molecular structures modeling (Blinn, 1982), or shape reconstruction (Keselman & Hebert, 2023). These representations can also be utilized in applications involving shadow (Nulkar & Mueller, 2001) and cloud rendering (Man, 2006). In addition, a new technique of 3D Gaussian Splatting (3D-GS) was recently introduced (Kerbl et al., 2023). This method couples splatting methods with point-based rendering for real-time rendering speed. The rendering quality of 3D-GS is comparable to that of Mip-NeRF (Barron et al., 2021), one of the best multilayer perceptron-based renderers.

The GS surpasses NeRF in terms of both training and inference speed, distinguishing itself by not depending on a neural network for operation. Rather, GS stores essential information within its 3D Gaussian components, a feature that renders it well-suited for dynamic scene modeling (Wu et al., 2023). Additionally, integrating GS with a dedicated 3D computer graphics engine is a straightforward process (Kerbl et al., 2023). However, conditioning GS is a challenging task due to the large number of Gaussian components typically involved, which can reach hundreds of thousands.

GaussianAvatars (Qian et al., 2023), utilizes the local coordinate system to generate Gaussians corresponding to the mesh’s faces. This approach is specifically designed for avatars and assumes the availability of a realistic (external) model for mesh fitting. However, training both the mesh and GS simultaneously is not feasible. While these solutions offer certain advantages, they do not directly combine Gaussian components with the mesh. As a result, automatic

adaptation of the Gaussian parameters to changing mesh is impossible.

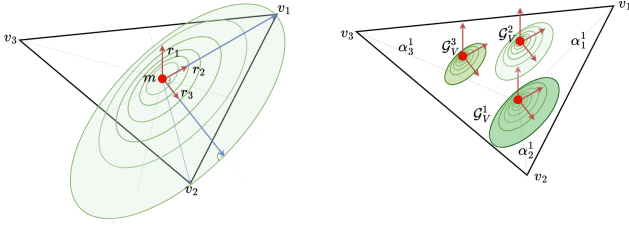


Figure 3. The left image presents the Gaussian component constructed on the face $V = \{\mathbf{v}_1, \mathbf{v}_2, \mathbf{v}_3\}$. We overlap the centers of Gaussian and face and parameterize the covariance matrix by vertices V . The right image presents how our model uses previously estimated Gaussian to construct k (in Figure $k = 3$) components in GS. GaMeS components are built by scaling and a translation on a mesh face.

The more advanced method is proposed by SuGaR (Guédon & Lepetit, 2023), which introduces a regularization term in the GS cost function to encourage alignment between the Gaussians and the surface of the scene. SuGaR achieves this by using signed distance functions (SDF) and minimizing the difference between the SDF and the computed Gaussian values. In SuGaR, the authors propose a method for extracting mesh from the GS model. They also introduce an optional refinement strategy that binds Gaussians to the surface of the mesh and jointly optimizes these Gaussians and the mesh through GS rendering.

In our work, we modify the third stage of the SuGaR model and show that it can be used as a separate method without expensive mesh initialization.

3. GaMeS: Mesh-Based Gaussian Splatting

This section delves into the details of the GaMeS model, commencing with the fundamental aspects of vanilla GS. Subsequently, we elucidate how we parameterize Gaussian distributions on the mesh’s faces. Finally, we introduce the novel GaMeS approach.

Gaussian Splatting The Gaussian Splatting (GS) technique captures a 3D scene through an ensemble of 3D Gaussians, each defined by its position (mean), covariance matrix, opacity, and color. Additionally, spherical harmonics (SH) are employed to depict the color attributes. (Fridovich-Keil et al., 2022; Müller et al., 2022). The GS effectiveness is primarily attributed to the rendering process, which utilizes projections of Gaussian components. GS relies on a dense set of 3D Gaussian components with color and opacity:

$$\mathcal{G} = \{(\mathcal{N}(\mathbf{m}_i, \Sigma_i), \sigma_i, c_i)\}_{i=1}^n,$$

where \mathbf{m}_i denotes position, Σ_i marks covariance, σ_i stands for opacity, and c is SH colors of i -th component.

The parameters of Gaussian distributions undergo direct training through gradient optimization. To enhance adaptability to complex scenes, GS employs additional training strategies. Notably, significant Gaussian components are subdivided. If the update parameters are substantial, Gaussians components are duplicated, which also can be removed due to their low transparency. In addition, the GS training procedure is implemented in the CUDA kernel, which supports fast training and real-time rendering.

Distribution on Mesh Faces In GaMeS, we placed all Gaussian components onto the mesh surface. Let us examine a single triangle face with vertices:

$$V = \{\mathbf{v}_1, \mathbf{v}_2, \mathbf{v}_3\} \subset \mathbb{R}^3.$$

We aim to parameterize the Gaussian components using vertices from the face V . We express the mean vector as a convex combination of vertices V , thus determining the Gaussian splats positions:

$$\mathbf{m}_V(\alpha_1, \alpha_2, \alpha_3) = \alpha_1 \mathbf{v}_1 + \alpha_2 \mathbf{v}_2 + \alpha_3 \mathbf{v}_3,$$

where $\alpha_1, \alpha_2, \alpha_3$ are trainable parameters such that $\alpha_1 + \alpha_2 + \alpha_3 = 1$. Through this parameterization, we consistently maintain the Gaussians positioned in the middle of the face V .

The covariance matrix can be defined as an empirical covariance calculated from three points. However, such a solution is complex to combine with the optimization proposed in GS. Instead, the covariance is parameterized by factorization:

$$\Sigma = R^T S S R,$$

where R is the rotation matrix and S the scaling parameters. Here, we define rotation and scaling matrices to stay in the original framework. Let start from orthonormal vectors: $\mathbf{r}_1, \mathbf{r}_2, \mathbf{r}_3 \in \mathbb{R}^3$, consisted into rotation matrix $R_V = [\mathbf{r}_1, \mathbf{r}_2, \mathbf{r}_3]$. Where the first vector is defined by the normal vector:

$$\mathbf{n} = \frac{(\mathbf{v}_2 - \mathbf{v}_1) \times (\mathbf{v}_3 - \mathbf{v}_1)}{\|(\mathbf{v}_2 - \mathbf{v}_1) \times (\mathbf{v}_3 - \mathbf{v}_1)\|},$$

where \times is the cross product. Given an explicitly defined mesh, we consistently possess knowledge of the vertex order for any given face. Hence, to calculate \mathbf{r}_2 , we define the vector from the center to the vertex \mathbf{v}_1 :

$$\mathbf{r}_2 = \frac{\mathbf{v}_1 - \mathbf{m}}{\|\mathbf{v}_1 - \mathbf{m}\|},$$

where $\mathbf{m} = \text{mean}(\mathbf{v}_1, \mathbf{v}_2, \mathbf{v}_3)$, which corresponds to the centroid of the triangle.

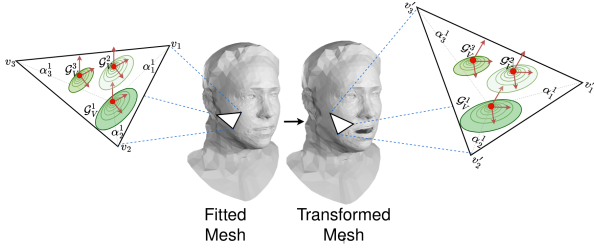


Figure 4. Visualization of affine transformation of Gaussian components when we modify mesh. Mesh vertices parameterize the mean and covariance matrix of Gaussian. Therefore, such parameters update when we change the mesh.

The last operation is obtained through orthonormalizing the vector with respect to the existing two vectors (a single step in the Gram–Schmidt process (Björck, 1994)):

$$\text{orth}(\mathbf{x}; \mathbf{r}_1, \mathbf{r}_2) = \mathbf{x} - \text{proj}(\mathbf{x}, \mathbf{r}_1) - \text{proj}(\mathbf{x}, \mathbf{r}_2),$$

where

$$\text{proj}(\mathbf{v}, \mathbf{u}) = \frac{\langle \mathbf{v}, \mathbf{u} \rangle}{\langle \mathbf{u}, \mathbf{u} \rangle} \mathbf{u}.$$

To obtain \mathbf{r}_3 , we use the vector from the center to the second vertex of the triangle:

$$\mathbf{r}_3 = \frac{\text{orth}(\mathbf{v}_2 - \mathbf{m}; \mathbf{r}_1, \mathbf{r}_2)}{\|\text{orth}(\mathbf{v}_2 - \mathbf{m}; \mathbf{r}_1, \mathbf{r}_2)\|}.$$

In consequence, we obtain a rotation matrix $R_V = [\mathbf{r}_1, \mathbf{r}_2, \mathbf{r}_3]$, which aligns with the triangular face. As scaling parameter S we use:

$$S_V = \text{diag}(s_1, s_2, s_3),$$

where $s_1 = \varepsilon$, $s_2 = \|\text{mean}(\mathbf{v}_1, \mathbf{v}_2, \mathbf{v}_3) - \mathbf{v}_1\|$, and $s_3 = \langle \mathbf{v}_2, \mathbf{r}_3 \rangle$. The first scaling parameters correspond with the normal vector. Since, in our case, the Gaussians are positioned on the faces, aligning with the surface s_1 should be equal to zero. To avoid numerical problems we fix this value as a small value (constant). On the other hand, s_2 and s_3 are proportional to distances from the center to the triangle border.

Consequently, the covariance of Gaussian distribution positioned to face is given by:

$$\Sigma_V = R_V^T S_V S_V R_V,$$

and correspond with the shape of a triangle V . Fig. 3 shows the process of determining Gaussians. Here the α_j^i refer to the i -th Gaussian \mathcal{G}_V^i , and the j -th vertex, respectively.

Within our model, we train a scale parameter, denoted as ρ , to dynamically adjust the Gaussian component size. For one face let us take $k \in \mathbb{N}$ number of Gaussians:

$$\mathcal{G}_V = \{\mathcal{N}(\mathbf{m}_V(\alpha_1^i, \alpha_2^i, \alpha_3^i), \rho^i \Sigma_V)\}_{i=1}^k,$$

where $\alpha_1^i + \alpha_2^i + \alpha_3^i = 1$ and $\rho^i \in \mathbb{R}_+$.

This distribution method enables us to render Gaussian splats solely dependent on the position of the mesh triangles. Consequently, we can readily perform geometric transformations when dealing with Gaussians within a single (triangle) face. Triangle transformation will apply Gaussian transformation as well. Such a novel approach is crucial to our work, and we can relate this to the *affine Gaussian transformation*.



Figure 5. GaMeS use a fixed number of faces. In the case of a mesh containing faces of different sizes, finding such parameters causes problems. In such a case, we propose to divide large faces into smaller parts. The left side includes only the original mesh, while on the right, the sizable mesh faces of the brown pool surrounding have been subdivided into smaller ones.

Fig. 4 shows examples of such transformation for rotation and scaling. Face V at time zero corresponds to the triangle $V = \{\mathbf{v}_1^V, \mathbf{v}_2^V, \mathbf{v}_3^V\}$, then it is transformed into $V' = \{\mathbf{v}_1^{V'}, \mathbf{v}_2^{V'}, \mathbf{v}_3^{V'}\}$. Three Gaussians splats $\mathcal{G}_V^1, \mathcal{G}_V^2, \mathcal{G}_V^3$ depend only on the position of the vertices.

GaMeS: Gaussian Splatting on Mesh The essential step in our model involves positioning Gaussians on the 3D mesh of the scene or object in question. This non-trivial approach disregards the hierarchy of Gaussian positions and facilitates ease of potential animation. Here, we have to consider two crucial experimental scenarios, namely, with and without using mesh during the training. First, we assume that a mesh is being provided and exclusively train the Gaussian components' centers, colors, and opacity. Second, we conduct training simultaneously on the mesh and Gaussian components. In the latter case, initialization of the mesh is required and achieved by utilizing points, for example, from the COLMAP tool and straightforward meshing strategies. We also show the initialization of the mesh using *Faces Learned with an Articulated Model and Expressions* (FLAME) (Li et al., 2017), i.e., a human face initialization. We adjust the mesh vertices and Gaussian parameters throughout the training process.

Let us consider a mesh denoted as $\mathcal{M} = (\mathcal{V}, \mathcal{E})$, where $\mathcal{V} \subset \mathbb{R}^3$ represents vertices, and $\mathcal{E} \subset \mathbb{R}^3$ signifies edges. The mesh's faces, denoted by $\mathcal{F}_{\mathcal{M}} = \left\{ \left(\mathbf{v}_1^{V_i}, \mathbf{v}_2^{V_i}, \mathbf{v}_3^{V_i} \right) \right\}_i^n$ are described by sets of vertices. As previously detailed,

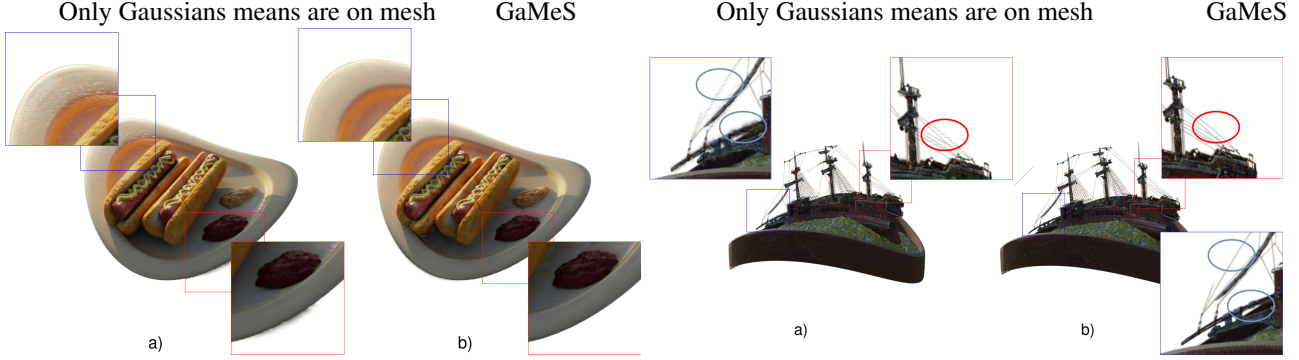


Figure 6. GaMeS parameterizes all Gaussian components by mesh vertices to lie directly on the mesh. Therefore, when we modify the mesh positions, we automatically adapt the components’ means and covariances. Consequently, we can see differences in the rendered image quality for the transforming when (a) only the Gaussian position is editable, and (b) when the Gaussian rotation and scaling are editable.

such mesh serves as a parameterization for shaping Gaussian components.

For our experiments, we choose the number $k \in \mathbb{N}$ of Gaussian components per mesh face and define how densely they should be placed on its surface. For mesh containing $n \in \mathbb{N}$ faces, the final number of Gaussians is fixed and equal to $k \cdot n$.

For each Gaussian component, we define trainable parameters used to calculate mean and covariance $\{(\alpha_1^i, \alpha_2^i, \alpha_3^i, \rho^i)\}_{i=1}^{k \cdot n}$. Therefore, GaMeS use a dense set $\mathcal{G}_{\mathcal{M}}$ of 3D Gaussians

$$\mathcal{G}_{\mathcal{M}} = \bigcup_{V_i \in \mathcal{F}_{\mathcal{M}}} \{\mathcal{G}_{V_i}, \sigma_{i,j}, c_{i,j}\}_{j=1}^k,$$

where $\sigma_{i,j}$ is opacity, and $c_{i,j}$ is SH colors of j -th Gaussian, and i -th face.

Mesh initialization During training, we can modify mesh vertices and Gaussian parameters. We can also use external tools for mesh fitting (Takikawa et al., 2021a) and train only Gaussian components. In the experimental section, we show both of such scenarios.

In our model, we use a fixed number of Gaussian components per face. In the case of models with various face sizes, finding such parameters is not trivial. To solve such a problem, we propose to divide large faces into smaller parts, see Fig. 5.

Mesh modification GaMeS parameterize all Gaussian components by vertices of mesh in such a way that they lie on meshes. Therefore, when we modify mesh positions, we automatically adapt the means and covariances of relevant Gaussians. Such an approach allows us to work with transformation. To better visualize such properties, we compare our model with a solution where the Gaussian components’

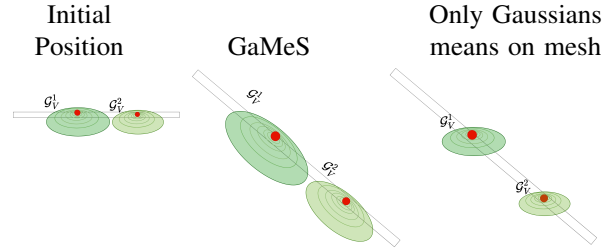


Figure 7. Compared to a method solely based on Gaussian averaging dependent on position, we observe that, following rotation and stretching the surface, Gaussians should dynamically adjust their scale and rotation to seamlessly conform to the change as in the case of GaMeS model.

centers are placed on mesh faces but do not parameterize the covariance matrix. Fig. 6 we can see that GaMeS Gaussian component adapts automatically to mesh modification.

In particular, when an object is bent, models that would only consider the position (means) of Gaussians depending on the mesh would fail to adapt properly. We can observe this effect in Fig. 6 with the ship’s rope rendering. In contrast, GaMeS, provides a perfect fit with the modification, and the operation scheme is shown in Fig. 7.

4. Experiments

Here, we delineate implementation details, describe the used datasets and the reasons for their selection. Then, we describe three scenarios: (1) when we have an existing mesh, (2) when we train mesh based on COLMAP initialization, and (3) when we use FLAME initialization. In the end, we show inference time both on static and animated scenes.

	PSNR \uparrow							
	Chair	Drums	Lego	Mic	Materials	Ship	Hotdog	Ficus
	Static							
NeRF	33.00	25.01	32.54	32.91	29.62	28.65	36.18	30.13
VolSDF	30.57	20.43	29.46	30.53	29.13	25.51	35.11	22.91
Ref-NeRF	33.98	25.43	35.10	33.65	27.10	29.24	37.04	28.74
ENVIDR	31.22	22.99	29.55	32.17	29.52	21.57	31.44	26.60
Plenoxels	33.98	25.35	34.10	33.26	29.14	29.62	36.43	31.83
Gaussian Splatting	35.82	26.17	35.69	35.34	30.00	30.87	37.67	34.83
	Editable							
GaMeS (our)	32.05	25.43	33.54	34.78	27.54	30.79	34.36	33.12
RIP-NeRF	34.84	24.89	33.41	34.19	28.31	30.65	35.96	32.23

Table 1. Quantitative comparisons (PSNR) on a NeRF-Synthetic dataset showing that GaMeS gives comparable results with other models.

	PSNR \uparrow									
	Outdoor scenes					Indoor scenes				
	bicycle	flowers	garden	stump	treehill	room	counter	kitchen	bonsai	
	Static									
Plenoxels	21.91	20.10	23.49	20.66	22.25	27.59	23.62	23.42	24.66	
INGP-Big	22.17	20.65	25.07	23.47	22.37	29.69	26.69	29.48	30.69	
Mip-NeRF360	24.37	21.73	26.98	26.40	22.87	31.63	29.55	32.23	33.46	
GS - 7K	23.60	20.52	26.25	25.71	22.09	28.14	26.71	28.55	28.85	
GS - 30K	25.25	21.52	27.41	26.55	22.49	30.63	28.70	30.32	31.98	
	Editable									
R-SuGaR-15K	22.91	-	25.29	24.55	-	29.95	27.47	29.38	30.42	
GaMeS (small) (Our)	22.32	19.18	25.93	24.26	21.56	28.49	25.88	25.92	26.98	
GaMeS (large) (Our)	23.46	19.39	26.28	24.59	21.40	28.83	26.44	27.18	27.84	

Table 2. The quantitative comparisons of reconstruction capability (PSNR) on Mip-NeRF360 dataset. R-SuGaR-15K uses 200K vertices. GaMeS (large) uses 30 Gaussians per face on mesh from COLMAP and 10 for mesh from GS. GaMeS (small) uses 10 Gaussians per face on mesh from COLMAP and 1 for mesh from GS.

4.1. Implementation details and data description

The time taken by the optimization process for our model varied from a few up to no more than sixty minutes, as it depends on factors like scene complexity, dataset characteristics, the number of Gaussians per face, and vertex fine-tuning decisions. Nonetheless, all experiments were conducted within a reasonable time frame, underscoring the efficiency of our approach across diverse scenarios. The supplementary material provides all the relevant details, and the source code is available in Github¹.

We illustrated the fundamental gains of GaMeS model through experiments with three distinct datasets.

Synthetic Dataset: A NeRF-provided eight geometrically complex objects with realistic non-Lambertian materials (Mildenhall et al., 2020). In addition to containing images of the objects, the dataset also incorporates corresponding meshes. We leveraged this dataset for our initial experiments to unequivocally showcase the capabilities of our model and underscore its flexibility in mesh editing.

Mip-NeRF360 Dataset: A dataset comprising five outdoor

¹<https://github.com/waczjoan/gaussian-mesh-splatting>

and four indoor scenes, each featuring intricate central objects or areas against detailed backgrounds (Barron et al., 2022). We used this dataset to demonstrate the adaptability of our model in handling dense scenes, employing a non-conventional strategy during the initial training stage in mesh preparation.

Human Faces Dataset: A modified subset of the Stirling/ESRC 3D Face Database², that includes images of six people, generated using *Blender* software from various perspectives, consistently excluding the backs of heads. Only one expression is assigned for each face. Notably, the dataset lacks corresponding mesh representations for the depicted person. This dataset is used to compare GaMeS with the NeRF_{flame} model (Zajac et al., 2023), mainly within the human-mesh fitting task.

4.2. Scenario I: Model with existing mesh

In this scenario, we utilize the provided mesh, incorporating Gaussians by strategically placing them onto its surface.

Our initial experiments used the Synthetic Dataset (Mildenhall et al., 2020), incorporating shared meshes. Table 1

²<https://pics.stir.ac.uk/ESRC/index.htm>

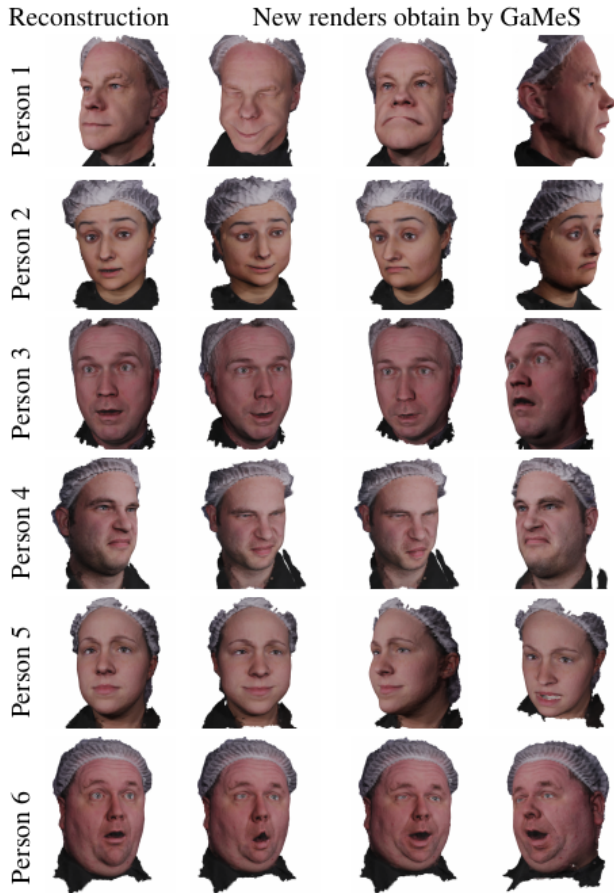


Figure 8. Reconstruction of 3D peoples and generation of new expressions using the GaMeS model.

presents PSNR metrics demonstrating the competitiveness of GaMeS approach with existing methods. Additional numerical comparisons are available in the supplementary material.

Notably, a significant contribution lies in the ease with which renders can be modified manually or in an automated process. Fig. 1 shows examples of reconstruction and simple object animations.

4.3. Scenario II: Joint training of mesh and GS

Our approach is capable of modeling unbounded scenes. In order to achieve that, we first create an initial mesh and then adjust it during the training. Results in Table 2 demonstrate that such modeling is feasible and reasonably comparable to other existing models. Particularly, the results show parity with the GS-7K and R-SuGaR-15K models.

It is important to highlight that the rendering quality is contingent upon the quality of the acquired mesh. In our experiments, we opted for a hybrid approach to generating

the initial mesh. This approach combines two meshes, each using a different number of Gaussian splats per face. The first mesh is extracted directly from the shared point cloud COLMAP, while the second mesh is inspired by the SuGaR technique (Guédon & Lepetit, 2023) and involves training GS over 7000 iterations to treat the 3D Gaussians positions as a point cloud. Only 20% of them are then transformed into a mesh using the *Alpha Shapes* (Edelsbrunner et al., 1983) algorithm.

As anticipated, we observe scene reconstruction, including both objects and details, see Fig. 2. Nevertheless, backgrounds and elements with large mesh faces may exhibit a lower-quality appearance. However, this does not hinder the feasibility of GaMeS model for reconstruction and modification. Additionally, the experiment revealed that Gaussian splats do not need to form a hierarchical structure. Instead, they can be embedded quite flatly, which is a non-trivial observation, and to our knowledge, it is not considered.

Numerous methods facilitate the generation of an initial mesh for objects, but our primary focus is not on this task. Instead, we emphasize addressing distinct issues that extend beyond the scope of initializing object meshes like EG3D (Chan et al., 2022), NGLoD (Takikawa et al., 2021b) or NeRFMeshing (Rakotosaona et al., 2023).



Figure 9. The main idea of fitting human mesh and how it can be transformed to a different person.

4.4. Scenario III: GaMeS with FLAME as Init Mesh

In this experiment, we show the possibility of fitting mesh using an *Init Mesh*, which was not acquired directly from our data in contrast to previous scenarios. Here, we relied on the Faces Dataset as it provides such required experimental data. To initialize the meshes, we used the FLAME (Li et al., 2017) framework, generating fully controllable meshes of human faces. Consequently, we could highlight the key advantage of GaMeS model, i.e., the ability to modify objects. We used the official implementation of the FLAME, with the number of parameters suggested in RingNet (Sanyal et al., 2019) In addition, we implemented an extra detail learning parameter to better represent hair or T-shirts.

Fig. 9, shows the main idea behind our approach. Initially, a human mesh is generated using the FLAME model. By accurately adjusting the mesh, we gain the ability to apply it, for example, to another person. By utilizing the

FLAME parameters, we can modify various aspects, especially facial expressions, to generate facial expressions like smiling, sadness, eye closure, mouth opening, and flirty or disgusted expressions. The possibilities of reconstruction and modifications for all six faces are depicted in Fig. 8. All expressions were chosen randomly as our main goal was to show GaMeS model’s ability to render objects as well as its modifications/animations.

Person	PSNR \uparrow					
	1	2	3	4	5	6
	Static					
NeRF	33.37	33.39	33.08	31.96	33.15	32.42
GS	50.16	49.04	49.81	49.97	49.77	49.17
	Editable					
NeRFlame	27.89	29.79	29.70	25.78	32.59	29.18
GaMeS	32.73	29.56	29.42	29.95	32.27	31.50

Table 3. Comparison of PSNR, SSIM, and LPIPS matrices between static models: NeRF, GS and referring to them: NeRFlame and GaMeS. We used 100 Gaussians per face.

The comparison of the mesh fitting capability between the GaMeS with the NeRFlame model is shown in Fig. 10. Notably, the faces are distinctly delineated and closely resemble the modeled objects, capturing not only postures but also expressions and intricate details.

Table 3 shows the results of using PSNR metrics on six faces. Comparisons are made between the two baseline NeRF models, GS, and the models created from them, i.e., the corresponding NeRFlame and GaMeS with animation capabilities.

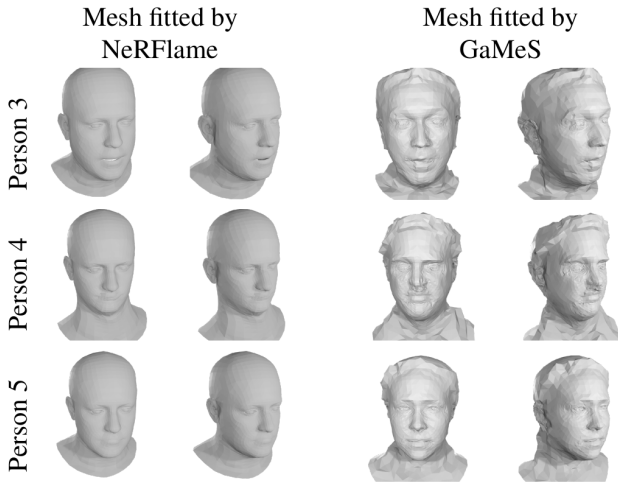


Figure 10. During the training of GaMeS, we simultaneously model FLAME mesh. Here, we present the meshes fitted by GaMeS compared to fitted mesh by NeRFlame model.

	FPS	GaMeS		GaMeS-A	
		Num. of comp.	PSNR	FPS	
bicycle	230	1 316 658	22.3		43.2
flowers	260	815 966	19.2		58.9
garden	163	2 092 692	25.9		31.9
stump	333	658 420	24.3		65.6
treehill	120	975 790	21.5		36.2
room	230	775 096	28.5		52.3
counter	213	502 808	25.9		60.0
kitchen	201	532 324	25.9		62.4
bonsai	174	1 274 648	27.0		42.4

Table 4. Comparison of achieved frame rate (FPS) on different scenes. GaMeS-A means FPS during modification. In each frame, we have different mesh positions. We can render static and dynamic scenes in real-time. All results were obtained using the RTX 4080 GPU.

4.5. Real-time rendering

We show that GaMeS can produce high-quality renders similar to GS or NeRF. Furthermore, we can manipulate mesh structures to obtain real-time modification of 3D objects, see Table 4. In our process of modification/simulation, we do not have any additional steps, which results in a considerable advantage of our approach.

To prove that, we conducted experiments to compare GS with GaMeS, examining their performance in static visualizations. We extend our experiments to include dynamic scenes by evaluating the performance of GaMeS in an animated scenario, see Fig. 2. By analyzing FPS metrics in static and animated contexts, we seek to provide real-time rendering. For comparability, all the computations were performed using the same RTX 4080 GPU.

5. Conclusion

This paper presents a new GS-based model called GaMeS that leverages two main concepts, i.e., classical mesh and vanilla GS. Here, we represent a 3D scene with a set of Gaussian components lying on the mesh. Moreover, we parameterize the Gaussian components by the mesh vertices, allowing single-stage training. In inference, we obtain GS, which can be modified in real time by manipulating mesh components. As a result, when the mesh changes, all Gaussian components automatically adapt to a new shape.

Limitations GaMeS allows real-time modifications, but artifacts appear in the case of significant changes in the case of meshes with large faces. In practice, large faces should be divided into smaller ones. How to change Gaussian components in GaMeS when mesh faces are split is not apparent.

Societal impact Our GaMeS contributes to lowering the computational complexity of 3D modeling, therefore reduc-

ing the energy consumption of such models.

References

- Barron, J. T., Mildenhall, B., Tancik, M., Hedman, P., Martin-Brualla, R., and Srinivasan, P. P. Mip-nerf: A multiscale representation for anti-aliasing neural radiance fields. In *Proceedings of the IEEE/CVF International Conference on Computer Vision*, pp. 5855–5864, 2021.
- Barron, J. T., Mildenhall, B., Verbin, D., Srinivasan, P. P., and Hedman, P. Mip-nerf 360: Unbounded anti-aliased neural radiance fields. *CVPR*, 2022.
- Björck, A. Numerics of Gram-Schmidt orthogonalization. *Linear Algebra and Its Applications*, 197:297–316, 1994.
- Blinn, J. F. A generalization of algebraic surface drawing. *ACM Transactions on Graphics (TOG)*, 1(3):235–256, 1982.
- Chan, E. R., Lin, C. Z., Chan, M. A., Nagano, K., Pan, B., Mello, S. D., Gallo, O., Guibas, L., Tremblay, J., Khamis, S., Karras, T., and Wetzstein, G. Efficient geometry-aware 3D generative adversarial networks. In *CVPR*, 2022.
- Eckart, B., Kim, K., Troccoli, A., Kelly, A., and Kautz, J. Accelerated generative models for 3D point cloud data. In *Proceedings of the IEEE Conference on Computer Vision and Pattern Recognition*, pp. 5497–5505, 2016.
- Edelsbrunner, H., Kirkpatrick, D., and Seidel, R. On the shape of a set of points in the plane. *IEEE Transactions on Information Theory*, 29(4):551–559, 1983.
- Fridovich-Keil, S., Yu, A., Tancik, M., Chen, Q., Recht, B., and Kanazawa, A. Plenoxels: Radiance fields without neural networks. In *CVPR*, pp. 5501–5510, 2022.
- Gao, K., Gao, Y., He, H., Lu, D., Xu, L., and Li, J. Nerf: Neural radiance field in 3d vision, a comprehensive review. *ArXiv*, abs/2210.00379, 2022.
- Guédon, A. and Lepetit, V. Sugar: Surface-aligned gaussian splatting for efficient 3d mesh reconstruction and high-quality mesh rendering. *arXiv preprint arXiv:2311.12775*, 2023.
- Kerbl, B., Kopanas, G., Leimkühler, T., and Drettakis, G. 3d gaussian splatting for real-time radiance field rendering. *ACM Transactions on Graphics*, 42(4), 2023.
- Keselman, L. and Hebert, M. Flexible techniques for differentiable rendering with 3D gaussians. *arXiv preprint arXiv:2308.14737*, 2023.
- Li, T., Bolkart, T., Black, M. J., Li, H., and Romero, J. Learning a model of facial shape and expression from 4D scans. *ACM Transactions on Graphics, (Proc. SIG-GRAPH Asia)*, 36(6):194:1–194:17, 2017.
- Man, P. Generating and real-time rendering of clouds. In *Central European seminar on computer graphics*, volume 1. Citeseer Castá-Papiernicka, Slovakia, 2006.
- Mildenhall, B., Srinivasan, P. P., Tancik, M., Barron, J. T., Ramamoorthi, R., and Ng, R. NeRF: Representing Scenes as Neural Radiance Fields for View Synthesis. In *ECCV*, 2020.
- Müller, T., Evans, A., Schied, C., and Keller, A. Instant neural graphics primitives with a multiresolution hash encoding. *ACM Transactions on Graphics (ToG)*, 41(4): 1–15, 2022.
- Nulkar, M. and Mueller, K. Splatting with shadows. In *Volume Graphics 2001: Proceedings of the Joint IEEE TCVG and Eurographics Workshop in Stony Brook, New York, USA, June 21–22, 2001*, pp. 35–49. Springer, 2001.
- Qian, S., Kirschstein, T., Schoneveld, L., Davoli, D., Giebenhain, S., and Nießner, M. GaussianAvatars: Photorealistic Head Avatars with Rigged 3D Gaussians. *arXiv preprint arXiv:2312.02069*, 2023.
- Rakotosaona, M.-J., Manhardt, F., Arroyo, D., Niemeyer, M., Kundu, A., and Tombari, F. NeRFMeshing: Distilling Neural Radiance Fields into Geometrically-Accurate 3D Meshes, 03 2023.
- Sanyal, S., Bolkart, T., Feng, H., and Black, M. Learning to regress 3d face shape and expression from an image without 3d supervision. In *Proceedings IEEE Conf. on Computer Vision and Pattern Recognition (CVPR)*, June 2019.
- Takikawa, T., Litalien, J., Yin, K., Kreis, K., Loop, C., Nowrouzezahrai, D., Jacobson, A., McGuire, M., and Fidler, S. Neural geometric level of detail: Real-time rendering with implicit 3D shapes. In *Proceedings of the IEEE/CVF Conference on Computer Vision and Pattern Recognition*, pp. 11358–11367, 2021a.
- Takikawa, T., Litalien, J., Yin, K., Kreis, K., Loop, C., Nowrouzezahrai, D., Jacobson, A., McGuire, M., and Fidler, S. Neural Geometric Level of Detail: Real-time Rendering with Implicit 3D Shapes. 2021b.
- Wu, G., Yi, T., Fang, J., Xie, L., Zhang, X., Wei, W., Liu, W., Tian, Q., and Wang, X. 4d gaussian splatting for real-time dynamic scene rendering. *arXiv preprint arXiv:2310.08528*, 2023.
- Zajac, W., Waczyńska, J., Borycki, P., Tabor, J., Zięba, M., and Spurek, P. NeRFflame: FLAME-based conditioning of NeRF for 3D face rendering. *arXiv preprint arXiv:2303.06226*, 2023.

A. Appendix

The appendix to the paper contains excerpts related to NeRF Synthetic and a continuation of the numerical results expounded in the main document.

A.1. Number of Gaussians per face

Here, we show the results of the experiments for the NeRF Synthetic dataset with a white background and original mesh. The dependence of the PSNR, SSIM and LPIPS result on the number of Gaussians per face is shown in Table 5.

Mostly, as a consequence of increasing the number of Gaussians, we get better results, and we can observe that a single Gaussian per face is insufficient. Materials and Lego has a very dense mesh, consequently positioning an excessive number of Gaussians within a confined space does not yield substantial improvements in the results.



Figure 11. A qualitative assessment delineating the impact of varying Gaussian quantities per face, discerned between the initial mesh and its subdivided counterpart.

However, experiments have shown that choosing a fixed number of Gaussians per face mesh is inefficient when the mesh contains different face sizes – in particular, it is difficult to cover large faces. Therefore, we decided to split the large facets. Splitting large facets, even using fewer Gaus-

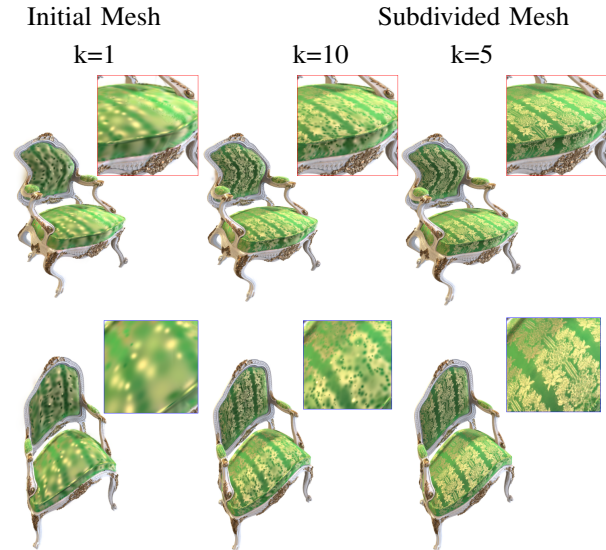


Figure 12. A juxtaposition of outcomes is conducted for a model varying in Gaussian counts per face and with a mesh subdivided. GaMeS with good mesh initialization is able to capture fine details.

sians per face, allows for significantly better results and detail capturing. The effects are shown in Fig. 11 (initial positions) and Fig. 12 (modifications).

A.2. Modification

Illustrating the reconstruction and modification through the application of the GaMeS model is shown in Fig. 13. GaMeS allows the creation of lifelike alterations, such as elevating the excavator blade or imaginative and surrealistic bends.

In fact, modification depends only on user skills. Fig. 14 shows various modifications of the ficus such as: a) scaling b) modifying a certain part – like bending branches, or modifying the whole object – dancing ficus. (c) ignoring a certain part. All images are generated from the view of the same camera. Note that Gaussians represent color from two sides. Therefore, after removing the soil from the pot, we can still see the inner side of the pot.

A.3. Extension of numerical results from main paper

Here, we present extensions of experiments proposed in the main part.

Number of Gaussians	PSNR \uparrow							
	Chair	Drums	Lego	Mic	Materials	Ship	Hotdog	Ficus
1	29.32	25.18	32.74	32.48	25.37	27.45	32.10	32.05
5	30.70	25.35	33.21	32.49	25.29	29.29	33.40	32.29
10	31.11	25.36	OOM	32.29	25.25	29.56	33.65	32.35
	SSIM \uparrow							
	Chair	Drums	Lego	Mic	Materials	Ship	Hotdog	Ficus
1	0.934	0.940	0.972	0.984	0.916	0.879	0.959	0.978
5	0.950	0.942	0.975	0.984	0.914	0.894	0.968	0.978
10	0.95	0.942	OOM	0.983	0.913	0.896	0.970	0.979
	LPIPS \downarrow							
	Chair	Drums	Lego	Mic	Materials	Ship	Hotdog	Ficus
1	0.066	0.052	0.027	0.012	0.060	0.133	0.062	0.018
5	0.050	0.049	0.022	0.012	0.061	0.107	0.042	0.018
10	0.044	0.049	OOM	0.12	0.063	0.102	0.038	0.019

Table 5. The quantitative comparisons (PSNR / SSIM / LPIPS) on Synthetic dataset with original meshes, with white background. OOM - CUDA out of memory. In this experiment we used Tesla V100-SXM2-32GB GPU.

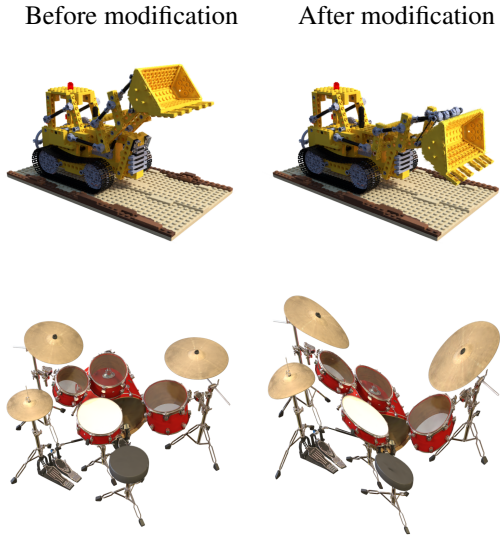


Figure 13. An example of reconstruction and modification using the GaMeS model. The model enables more realistic modifications like lifting the excavator blade as well as surrealistic drums bending.



Figure 14. Demonstrations of potential modifications facilitated by games include: a) scaling, b) transforming either specific components or entire objects, and c) selectively disregarding specific sections.

	PSNR \uparrow									
	Outdoor scenes					Indoor scenes				
	bicycle	flowers	garden	stump	treehill	room	counter	kitchen	bonsai	
	Static									
Plenoxels	21.91	20.10	23.49	20.66	22.25	27.59	23.62	23.42	24.66	
INGP-Big	22.17	20.65	25.07	23.47	22.37	29.69	26.69	29.48	30.69	
Mip-NeRF360	24.37	21.73	26.98	26.40	22.87	31.63	29.55	32.23	33.46	
GS - 7K	23.60	20.52	26.25	25.71	22.09	28.14	26.71	28.55	28.85	
GS - 30K	25.25	21.52	27.41	26.55	22.49	30.63	28.70	30.32	31.98	
	Editable									
R-SuGaR-15K	22.91	-	25.29	24.55	-	29.95	27.47	29.38	30.42	
GaMeS (Our)	23.46	19.39	26.28	24.59	21.40	28.83	26.44	27.18	27.84	
	SSIM \uparrow									
	Outdoor scenes					Indoor scenes				
	bicycle	flowers	garden	stump	treehill	room	counter	kitchen	bonsai	
	Static									
Plenoxels	0.496	0.431	0.606	0.523	0.509	0.842	0.759	0.648	0.814	
INGP-Big	0.512	0.486	0.701	0.594	0.542	0.871	0.817	0.858	0.906	
Mip-NeRF360	0.685	0.583	0.813	0.744	0.632	0.913	0.894	0.920	0.941	
GS - 7K	0.675	0.525	0.836	0.728	0.598	0.884	0.873	0.900	0.910	
GS - 30K	0.771	0.605	0.868	0.775	0.638	0.914	0.905	0.922	0.938	
	Editable									
R-SuGaR-15K	0.631	-	0.771	0.681	-	0.909	0.890	0.907	0.933	
GaMeS(Our)	0.669	0.460	0.831	0.660	0.611	0.892	0.844	0.861	0.887	
	LPIPS \downarrow									
	Outdoor scenes					Indoor scenes				
	bicycle	flowers	garden	stump	treehill	room	counter	kitchen	bonsai	
	Static									
Plenoxels	0.506	0.521	0.386	0.503	0.540	0.419	0.441	0.447	0.398	
INGP-Big	0.446	0.441	0.257	0.421	0.450	0.261	0.306	0.195	0.205	
Mip-NeRF360	0.301	0.344	0.170	0.261	0.339	0.211	0.204	0.127	0.176	
GS - 7K	0.318	0.417	0.153	0.287	0.404	0.272	0.254	0.161	0.244	
GS - 30K	0.205	0.336	0.103	0.210	0.317	0.220	0.204	0.129	0.205	
	Editable									
R-SuGaR-15K	0.349	-	0.218	0.336	-	0.243	0.234	0.166	0.219	
GaMeS(Our)	0.326	0.481	0.142	0.347	0.384	0.257	0.294	0.218	0.287	

Table 6. The quantitative comparisons (PSNR / SSIM / LPIPS) on the Mip-NeRF360 dataset. R-SuGaR-15K, with the number of 200K vertices.

	PSNR \uparrow							
	Chair	Drums	Lego	Mic	Materials	Ship	Hotdog	Ficus
Static								
NeRF	33.00	25.01	32.54	32.91	29.62	28.65	36.18	30.13
VolSDF	30.57	20.43	29.46	30.53	29.13	25.51	35.11	22.91
Ref-NeRF	33.98	25.43	35.10	33.65	27.10	29.24	37.04	28.74
ENVIDR	31.22	22.99	29.55	32.17	29.52	21.57	31.44	26.60
Plenoxels	33.98	25.35	34.10	33.26	29.14	29.62	36.43	31.83
Gaussian Splatting	35.82	26.17	35.69	35.34	30.00	30.87	37.67	34.83
Editable								
GaMeS (our)	32.05	25.43	33.54	34.78	27.54	30.79	34.36	33.12
RIP-NeRF	34.84	24.89	33.41	34.19	28.31	30.65	35.96	32.23
SSIM \uparrow								
Static								
NeRF	0.967	0.925	0.961	0.980	0.949	0.856	0.974	0.964
VolSDF	0.949	0.893	0.951	0.969	0.954	0.842	0.972	0.929
Ref-NeRF	0.974	0.929	0.975	0.983	0.921	0.864	0.979	0.954
ENVIDR	0.976	0.930	0.961	0.984	0.968	0.855	0.963	0.987
Plenoxels	0.977	0.933	0.975	0.985	0.949	0.890	0.980	0.976
Gaussian Splatting	0.987	0.954	0.983	0.991	0.960	0.907	0.985	0.987
Editable								
GaMeS (our)	0.976	0.945	0.973	0.986	0.928	0.895	0.977	0.979
RIP-NeRF	0.980	0.929	0.977	0.962	0.943	0.916	0.963	0.979
LPIPS \downarrow								
NeRF	0.046	0.091	0.050	0.028	0.063	0.206	0.121	0.044
VolSDF	0.056	0.119	0.054	0.191	0.048	0.191	0.043	0.068
Ref-NeRF	0.029	0.073	0.025	0.018	0.078	0.158	0.028	0.056
Plenoxels	0.031	0.067	0.028	0.015	0.057	0.134	0.037	0.026
ENVIDR	0.031	0.080	0.054	0.021	0.045	0.228	0.072	0.010
Gaussian Splatting	0.012	0.037	0.016	0.006	0.034	0.106	0.020	0.012
Editable								
GaMeS (our)	0.019	0.046	0.025	0.013	0.061	0.096	0.0258	0.020
RIP-NeRF	-	-	-	-	-	-	-	-

Table 7. Quantitative comparisons (PSNR) on a NeRF-Synthetic dataset showing that GaMeS gives comparable results with other models.